Dental Materials 40 (2024) 1909–1919

Contents lists available at ScienceDirect

Dental Materials

journal homepage: www.elsevier.com/locate/dental

Effect of the anti-Alzheimer drug GSK-3β antagonist on numerical modeling of the energy dissipation through the resin-dentin interface

Manuel Toledano [a], Enrique Fernández-Romero [a,b], Estrella Osorio [a,*], Fátima S. Aguilera [a], Christopher D. Lynch [c], María T. Osorio [a], Raquel Toledano [a], Raquel Osorio [a]

[a] University of Granada, Faculty of Dentistry, Colegio Máximo de Cartuja s/n, 18071 Granada, Spain
[b] Medicina Clínica y Salud Pública PhD Programme, University of Granada, 18071 Granada, Spain
[c] University Dental School & Hospital/Cork University Dental School & Hospital, Cork, Ireland

ARTICLE INFO

Keywords:
Mineralized dentin
Tideglusib
Nano-DMA
Nanoparticles
Atomic Force Microscopy. Stress concentration
Complex modulus
Tan delta

ABSTRACT

Objectives: The aim of this study was to determine the viscoelastic performance and energy dissipation of conditioned dentin infiltrated with polymeric nanoparticles (NPs) doped with tideglusib (TDg) (TDg-NPs).
Methods: Dentin conditioned surfaces were infiltrated with NPs and TDg-NPs. Bonded interfaces were created, stored for 24 h and submitted to mechanical and thermal challenging. Resin-dentin interfaces were evaluated through nano-DMA/complex-loss-storage moduli-tan delta assessment and atomic force microscopy (AFM) analysis.
Results: Dentin infiltrated with NPs and load cycled attained the highest complex modulus at hybrid layer and bottom of hybrid layer. Intertubular dentin treated with undoped NPs showed higher complex modulus than peritubular dentin, after load cycling, provoking energy concentration and breakdown at the interface. After infiltrating with TDg-NPs, complex modulus was similar between peri-intertubular dentin and energy dissipated homogeneously. Tan delta at intertubular dentin was higher than at peritubular dentin, after using TDg-NPs and load cycling. This generated the widest bandwidth of the collagen fibrils and bridge-like mineral structures that, as sight of energy dissipation, fastened active dentin remodeling. TDg-NPs inducted scarce mineralization after thermo-cycling, but these bridging processes limited breakdown zones at the interface.
Significance: TDg-based NPs are then proposed for effective dentin remineralization and tubular seal, from a viscoelastic approach.

1. Introduction

The guarantee of a correct adhesion to dentin is the formation of an adequate hybrid layer (HL). The HL is formed when the mineral component from the dentin has been removed and the adhesive resin has been infiltrated undergoing complete in situ polymerization [1]. Hence, a three-dimensional collagen-resin biopolymer is created, facilitating a linkage between the dentin substrate and the adhesive [2]. Nevertheless, after demineralization and further resin infiltration, a volume of unprotected collagen is generated at the bottom of the hybrid layer (BHL) [3]. This collagen is vulnerable to the action of matrix metalloproteinases (MMPs) [4–6], causing degradation and jeopardizing the longevity of bonded restorations [7,8]. Thus, remineralization of the unprotected collagen has pivotal implications in the improvement of bonding features. Thereby, a refined adhesive formulation for minimally invasive dentistry has to offer a durable and stronger adhesion to dental tissues. This biomaterial should also promote remineralization and protection of the interface by deploying bioactivity, even more in challenging conditions [9], as mechanic and thermal cyclic fatigue under functional stress [10].

Classical bioactive materials for functionalization of adhesives raise concerns respect to the regrowth of minerals at the demineralized dentin [11]. Engineered polymeric and hydrophilic nanoparticles (NPs) have been proposed as carriers of some biological factors to manage dentin remineralization [12]. In addition, Neves et al. (2017) [13], have proposed a biologically oriented methodology for dentin generation and remineralization. They reported the performance of the glycogen-synthase-kinase 3 (GSK-3) peptide in remineralization. GSK-3 phosphorylates Axin and β-catenin (β-cat), being a capital intracellular constituent of the Wnt/β-cat signaling pathway. Tideglusib (TDg), used

* Correspondence to: University of Granada, Faculty of Dentistry, Dental Materials Section, Colegio Máximo de Cartuja s/n, 18071 Granada, Spain.
E-mail address: meosorio@ugr.es (E. Osorio).

https://doi.org/10.1016/j.dental.2024.09.005
Received 25 June 2024; Received in revised form 10 September 2024; Accepted 10 September 2024
Available online 13 September 2024

in the treatment of Alzheimer's disease, as GSK-3 inhibitor, was postulated as a dentin repair therapy [14]. In the present research, the in vitro viscoelastic mechanical behavior of polymeric NPs serving as TDg carriers will be assessed, at the resin-dentin interface.

The mechanical performance of the dentin structure will be affected by the quality and the degree of the mineralization [15]. The precipitation of minerals at the intrafibrillar compartment of the demineralized collagen at the resin-dentin interface [16] is directly related to an increase of the mechanical properties [15,17]. One of the most commonly means of testing the mechanical behavior of substrates or materials [18], is the atomic force microscopy (AFM) nano-indentation. AFM represents, at nanoscale [19], a suitable method for the determination of the viscoelasticity of hard tissues [15,20]. The nano-dynamic mechanical analysis (nano-DMA) has demonstrated that the dampening (or viscous) behavior of dentin is highly sensitive to the structural changes that appear with the oral function [21].

The storage (elastic) and loss (damping) moduli are two modulus components of the complex modulus [22]. The ability to store energy by the sample during a cycle of loading [23] is characterized by the storage modulus (E') (also called dynamic stiffness), which is then available for elastic recoil. The ability of the material to dissipate energy is characterized by the loss modulus (E''). Stiffness and damping are measured by DMA. The tan delta (δ) is the ratio of the loss to the storage. The load cycling of the masticatory function significantly influences the interactions between restorative materials and dental tissues. The bonded interface should support and dissipate this energy, which is transmitted by the forces. Discrepancies in viscoelastic properties values within the distinct structures located within the resin-dentin interface pose a risk for cracking and breakdown. In relatively high elastic modulus regions, low modulus regions provoke stress concentration [2], accounting for catastrophic failures of the restored teeth. Peritubular (PD) and intertubular dentin (ID) represent two phases with a pivotal role in viscolestic properties of dentin. Both morpho and nanomechanical properties can be obtained by integrating nano-DMA and AFM [24].

The aim of the current research was to infiltrate tideglusib-loaded nanoparticles into phosphoric acid conditioned dentin, before the application of the adhesive resin, in order to evaluate a potential improvement of viscoelasticity after mineral precipitation at the resin-dentin interface submitted to thermal and mechanical loading. The null hypotheses to be tested are that tideglusib loaded nanoparticles infiltration into conditioned dentin, (1) does not affect the dynamic mechanical behavior at the resin-dentin interface, after thermal or mechanical challenging, (2) does not facilitate remineralization at the demineralized bonded interface, and (3) morphological characteristics at the resin dentin interface do not differ after infiltration of tideglusib-loaded nanoparticles.

2. Material and methods

2.1. Production of nanoparticles

The process of obtaining NPs applied the use of the polymerization precipitation method, which controlled the precipitation facilitated by a thermodynamic approach. Specifically, the Flory-Huggins model, based on Hansen's solubility parameters, was employed. This model centered on interactions among solvent molecules and the growth of polymer chains through hydrogen, polar bonding, and dispersion forces [25]. The backbone monomer for NP design was 2-hydroxyethyl methacrylate, with methacrylic acid serving as the functional monomer, and ethylene glycol dimethacrylate employed as the cross-linker. Subsequently, half of the produced NPs were loaded with a peptide, tideglusib (Sigma-Aldrich, Chemie GmbH, Riedstr, Germany). The NPs loading process was conducted by immersion of 100 mg of NPs in 1 mL of 0.0017 mg/mL TDg solution for 2 h at room temperature under constant shaking (12 rpm) (rotator Orbit 300445, JP Selecta, Barcelona, Spain). Then, the NPs were left until the solvent was completely evaporated, ensuring that all the TDg remains onto the NPs. Two types of NPs were obtained, undoped NPs and TDg-NPs.

2.2. Preparation of specimens for the bonding procedure, mechanical and thermal challenging

Thirty-six unerupted human third molars, preserved at 4ºC in a 0.5% chloramine T solution for no more than a month, were utilized for this study. Prior to their involvement, subjects provided informed consent, aligning with the Declaration of Helsinki and adhering to good clinical practice guidelines. The study received ethical approval from the local Ethics Committee (1906/CEIH/2020).

The teeth were horizontally sectioned just below the dentin-enamel junction to expose sound dentin surfaces. These surfaces were then flatly polished to create a clinically relevant smear layer, utilizing 180-grit silicon carbide –SiC- abrasive paper. Subsequently, the dentin surfaces underwent etching (with 37% phosphoric acid, during 15 s), followed by rinsing and drying. Random allocation of experimental teeth (n = 12) to one of three groups was achieved through computer-generated randomization, facilitated by http://www.randomizer.org/form.htm. The allocation remained concealed in sealed envelopes until the time of bonding procedure. Just an ethanol solution was applied (30 s) (i), or an ethanol suspension of undoped NPs (ii), and TDg-NPs (iii) (10 mg/mL) in each of the three experimental groups (n = 12), acting as primers. Ethanol was then evaporated for 30 s and, finally, Single Bond (SB) resin (3 M ESPE, St. Paul, MN, USA) was applied according to the manufacturer's instructions, to fulfill the conventional adhesive protocol. The sample preparation was conducted by one researcher, and a uniform adhesion protocol was implemented by a different researcher. For each tooth, a composite build-up (5 mm high) (Tetric EvoCeram, Ivoclar-Vivadent, Schaan, Liechtenstein) was performed using the incremental technique, in five 1 mm resin layers. The light-curing process was carried out with a Bluephase® polywave light-emitting diode light-polymerizing unit (Bluephase G2, Ivoclar Vivadent AG, Schaan, Liechtenstein) at 1500 mW/cm^2 for 20 s. The output intensity was monitored with a curing radiometer (Model Bluephase® meter, Ivoclar Vivadent AG, Schaan, Liechtenstein), ensuring a minimal output intensity of 1500 mW/cm^2 for all experiments. The restored teeth were stored in a dark environment and submerged in simulated body fluid solution (SBFS) for 24 h.

The specimens, within each experimental group, were then divided into three sub-groups (n = 4) based on the challenging method: (1) Restored teeth stored in SBFS for 24 h, (2) load cycling with a sine wave form for 24 h (259,200 cycles, 3 Hz) (S-MMT-250NB; Shimadzu, Tokyo, Japan) proceeding as in Sauro *et al.* 2009 [26], and (3) thermal cycling (100,000 cycles/ 5ºC and 55ºC) (SD Mechatronik GmbH, Germany) during approximately three months in distilled water [14]. Finally, the samples were sectioned into resin–dentin slabs and polished using ascending grit SiC abrasive papers (#1200 to #4000) on a water-cooled polishing device (Buehler-MetaDi, Buehler Ltd. Lake Bluff, IL, USA). The specimen preparation was concluded with a final ultrasonic cleaning (5 min). A schematic representation of the final resin-dentin interface is provided in the Fig. S1.

2.3. Nano-DMA analysis

Four resin-dentin slabs from each treated dentin were submitted for nano-DMA and AFM analysis in hydrated conditions. Property mappings were conducted using a Ti-750D (Hysitron, Inc., Minneapolis, MN) equipped with nano-DMA III, a commercial nano-DMA package. The indenter tip was calibrated against a fused quartz sample using a quasistatic force setpoint of 5μN to maintain contact between the tip and the sample surface. A dynamic (oscillatory) force of 5μN was superimposed on the quasistatic signal at a frequency of 200 Hz. Based on a calibration modulus of the tip value of 1.1400E+ 3 N/mm^2 for the fused quartz, the best-fit spherical radius approximation for tip was found to be 150 nm,

for the selected nano-DMA scanning parameters. Modulus mapping of our samples was conducted by imposing a quasistatic force setpoint, F_q= 5μN, to which we superimposed a sinusoidal force of amplitude F_A = 1.8μN and frequency f = 200 Hz.

Under steady conditions (application of a quasistatic force) the indentation modulus of the tested sample, E, was obtained by application of different models that relate the indentation force, F, and depth D [27]. Most of these theories assume proportionality between the force and the indentation modulus:

$$F = g(D)E \quad \rightarrow E = \frac{F}{g(D)} \tag{1}$$

Where g (D) is a function on the indentation depth, which depends on the geometry of the probe of the indenter. For example, for a spherical probe, the Hertzian contact theory predicts [27,28]:

$$g \quad (D) = \quad \frac{4R^{1/2} \quad D^{3/2}}{3(1 - \quad \nu^2)} \tag{2}$$

In this equation R is the radius of the spherical probe and v is the Poissonś ration of the tested sample. As mentioned above, in nano-DMA experiments an oscillatory force is superimposed to a quasistatic force:

$$F = \quad F_q + \quad F_A \quad \sin(2\pi ft) \tag{3}$$

With t being the time. Under this imposed force, the indentation depth takes the following form:

$$D = \quad D_q \quad + \quad D_A \quad \sin \quad (2\pi ft - \delta) \tag{4}$$

This means that the indentation depth also oscillates around a quasistatic value, with the same frequency that the oscillating force and delayed by a phase lag δ. In the limit of $F_A << F_q$ it can be expanded the Eq. (1) to a first order Taylor approximation, to obtain:

$$F_q + F_A \sin(2\pi ft) = g(D_q)E + g'(D_q)|E^*| \quad D_A \sin(2\pi ft - \delta). \tag{5}$$

In this equation, g´is the first derivate of g, and E * is the complex dynamic indentation modulus. Now, it can be equaled the time-dependent terms and change the time origin, to write:

$$F_A \sin(2\pi ft + \delta) = g(D_q')|E^*|D_A \sin(2\pi ft) \tag{6}$$

Now, the oscillating force can be decomposed into two terms, the in-phase term, F´, and the out-of-phase term, F˝ [29].

$$\begin{aligned} F_A \sin(2\pi ft + \delta) = & \quad F_A \quad \cos\delta \sin(2\pi ft) + F_A \sin\delta \cos(2\pi ft) \\ = & \quad F_A' \sin(2\pi ft) + \quad F_A'' \cos(2\pi ft) = F' + F'' \end{aligned} \tag{7}$$

Then, from this decomposition two dynamics moduli can be extracted:

$$E' = \quad |E^*|\cos\delta \quad = \quad \frac{F_A \cos\delta}{g(D_q')D_A} = \quad \frac{F_A'}{g(D_q')D_A} \tag{8}$$

Which is the in-phase or storage (elastic) modulus.

$$E'' = \quad |E^*|\sin\delta = \quad \frac{F_A \quad \sin\delta}{g(D_q') \quad D_A} \quad = \quad \frac{F_A''}{g(D_q') \quad D_A} \tag{9}$$

which is the out-phase or loss (viscous) modulus. Note the position of the phase lag, δ, in these equations. As mentioned above, these coefficients are directly related with measured parameters, without any particular assumption, except the consideration of the system consisting of the sample and the instrument tip as a driven simple oscillating under stationary conditions. From the application of different models relating indentation force (F) and depth (D), the indentation modulus of the tested sample (E) under application of a quasi-static force (stable conditions) was obtained [27].

The dentin discs were then removed from the SBFS immersion and scanned under hydrated conditions. To eliminate problems associated to the meniscus forces transferred from fluid droplets to the indenter [30], and to preserve hydration of the dentin surfaces, a drop (1.5 mL) of 99.4 % ethylene glycol [31] was applied on the polished surface of the specimen. For each dentin disc, three modulus mappings were recorded. Data from regions approximately 30 × 30 μm in size were collected using a scan rate of 0.2 Hz. Each scan resulted in a 256 × 256 pixel data array.

For each mapping and for each type of resin-dentin interface, 15 value points of complex modulus (E *), storage modulus (E'), loss modulus (E'') and tan delta (δ) were acquired for each zone of the interface, excluding the adhesive resin, i.e, hybrid layer (HL), bottom of hybrid layer BHL), intertubular dentin (ID) and peritubular dentin (PD) (Fig. S1).

2.4. Atomic Force Microscopy (AFM) analysis, collagen fibril diameter

For the topographical mapping, an atomic force microscope (AFM Nanoscope V, Digital Instruments, Veeco Metrology group, Santa Barbara, CA, USA) was employed, in this study, for surface analysis of the same samples. The imaging process was undertaken using a taping mode with an oscillating cantilever calibrated vertical-engaged piezo-scaner (Digital Instrument, Santa Barbara, CA, USA). A 10 nm radius silicon nitride tip (Veeco) was mounted at the end of an oscillating cantilever that came into intermittent contact with the surface at the lowest oscillation point. Vertical modifications of the AFM tip with a resonance frequency close to 330 kHz resulted in the height of the images shown as dark and bright zones. With a slow scan rate (0.1 Hz), digital images (2 ×2 μm) were captured for each dentin surface. To facilitated dentin surfaces observation, AFM images were tilted using a specific software (Nanoscope Analysis v. 1.40, Bruker Corporation, Billerica, MA, USA). To observe the fibril width of all groups, 5 random images (2 ×2 μm) were recordered from the samples. Collagen fibril diameter (in nanometers) were determined from the images by section analysis with data that were modified only by plane-fitting. The collagen fibril diameter was preferentially determined from fibrils that were exposed along their complete widths. Five fibrils and their interfibrillar spacings were analyzed from each image. Measurements were corrected for tip-broadening [32] by the equation $e = 2r$, where e is the error in the horizontal dimension and r is the tip's radius [33].

2.5. Statistical methods

Numerical data were further analyzed by ANOVA and Student-Newman-Keuls multiple comparison tests, with $p < 0.05$ as statistical significance. The validity of the assumptions of normality and homoscedasticity of the data had been previously verified.

3. Results

3.1. Nano-DMA analysis

Concerning the type of challenging within each group (capital letters in Table 1), at the hybrid layer, the highest E * was obtained at dentin infiltrated with undoped NPs load cycled, and dentin infiltrated with TDg-NPs load cycled. The control group thermo-cycled showed the lowest E * . In general, loss modulus, E'', performed similar regardless the type of NPs. The lowest E'' was obtained in the control specimens thermo-cycled. Dentin specimens treated with undoped NPs and mechanically loaded showed the highest E' among samples of this group. Specimens treated with TDg-NPs and thermo-cycled attained the highest storage modulus E' among samples of this group (Table 1). Tan (δ) practically performed similar in all groups (Table 1). At the bottom of the hybrid layer, the highest E * was obtained at dentin infiltrated with undoped NPs and load cycled, and dentin infiltrated with TDg-NPs load cycled. The property map of the interface promoted by demineralized dentin infiltrated with undoped NPs and TDg-NPs, both load cycled,

Table 1
Mean and SD of Complex, Loss, Storage Modulus (GPa) and Tan (δ) attained from experimental interfaces after 24 h, load cycling (LC) and thermo-cycling (TC).

	CONTROL			UNDOPED-NPs			TIDEGLUSIB-NPs		
	24 H	LC	TC	24 H	LC	TC	24 H	LC	TC
HYBRID LAYER									
E *	45.79 (6.34)Aa1	56.48 (11.89)Aa1	40.87 (3.73)Aa1	64.65 (16.77)Aa1	119.05 (27.27)Bb12	56.63 (13.20)Aa1	51.31 (8.92)Aa1	151.71 (30.94)Bb1	100.69 (13.17)Cb1
E ”	4.73 (6.22)Aa1	3.70 (2.93)Aa1	1.20 (1.28)Aa1	6.09 (1.82)Aa2	5.64 (4.79)Aa1	3.20 (2.26)Aa1	4.96 (4.84)Aa1	5.66 (2.49)Aa1	4.06 (2.98)Aa12
E´	44.10 (6.45)Aa1	55.67 (6.11)Ba1	40.32 (8.14)Aa2	50.71 (9.03)Aa2	194.21 (60.88)Bb1	48.52 (9.40)Aa1	50.20 (11.48)Aa1	45.60 (16.48)Aa1	151.62 (61.24)Bb2
Tan (δ)	–	0.18 (0.10)Aa1	0.09 (0.04)Aa1	0.22 (0.06)Aa2	0.12 (0.11)Aa1	0.20 (0.09)Aa1	0.17 (0.11)Aa1	0.18 (0.10)Aa1	0.26 (0.33)Aa12
BOTTOM OF HYBRID LAYER									
E *	61.07 (5.81)Aa2	53.93 (3.81)Aa1	43.26 (5.97)Ba1	44.15 (8.16)Ab11	156.79 (51.02)Bb12	62.08 (10.76)Ab1	117.08 (26.93)Ac2	185.22 (37.70)Bb1	83.37 (19.75)Ab1
E”	6.72 (5.17)Aa1	5.91 (6.34)Aa1	1.31 (1.97)Aa1	11.04 (4.57)Aa2	9.41 (4.56)Aa1	6.19 (0.98)Ab2	5.69 (4.59)Aba1	11.96 (2.73)Aa2	5.87 (3.19)Ab12
E´	63.89 (19.74)Aa12	53.89 (10.04)Aa1	45.69 (7.00)Aa2	30.21 (8.69)Ab1	139.27 (43.32)Bb1	55.07 (6.32)Ca1	115.67 (39.13)Ac2	210.27 (41.07)Bb2	45.67 (8.48)Ca1
Tan (δ)	–	0.30 (0.15)Aa1	0.07 (0.03)Ba1	0.24 (0.04)Aa2	0.16 (0.16)Aa1	0.24 (0.09)Ab1	0.18 (0.19)Aa1	0.26 (0.05)Aa1	0.49 (0.23)Ab2
INTERTUBULAR DENTIN									
E *	82.45 (9.21)Aa3	57.31 (11.24)Ba1	53.85 (13.42)Ba1	86.57 (12.85)Aa2	87.62 (21.09)Aab1	73.95 (13.60)Aa12	119.84 (34.33)Aa2	106.73 (36.64)Ab1	111.73 (30.85)Aa1
E”	5.45 (5.65)Aab1	3.17 (3.79)Aa1	3.36 (1.12)Aa2	16.44 (7.11)Aa2	11.58 (6.70)Aa1	7.82 (6.72)Aa12	3.97 (2.90)Ab1	10.14 (7.70)Aa2	7.52 (1.92)Aa2
E´	74.26 (22.02)Aa2	63.71 (20.02)Aa1	51.34 (11.15)Aa23	83.90 (22.76) Aa2	78.36 (18.69)Aa2	68.62 (9.31)Aab1	99.12 (43.89)Aa12	68.93 (13.16)Aa1	90.40 (21.55)Ab2
Tan (δ)	–	0.18 (0.15)Aa1	0.22 (0.10)Aa12	0.26 (0.11)Aa2	0.24 (0.11)Aa1	0.27 (0.10)Aa1	0.22 (0.11)Aa1	0.26 (0.09)Aa1	0.22 (0.20)Aa12
PERITUBULAR DENTIN									
E *	80.17 (15.15)Aa3	55.13 (9.65)Ba1	54.38 (11.41)Ba1	128.50 (13.83)Ab3	134.49 (21.65)Ab2	102.71 (17.00)Ab3	131.89 (19.74)Ab2	119.96 (35.40)Ab1	126.42 (34.10)Ab1
E”	48.49 (13.36)Aa2	27.87 (8.04)Aab2	23.34 (0.95)Aa1	30.99 (0.71)Aa3	27.57 (5.15)Aa2	27.93 (5.06)Aa3	10.72 (4.27)Ab	14.78 (5.13)Ab2	11.19 (1.57)Ab3
E´	133.50 (15.09)Aa3	118.50 (24.42)Aa2	98.83 (39.84)Aa3	120.27 (15.25)Aa2	107.94 (9.92)Aa2	98.57 (11.27)Aa2	171.30 (41.74)Aa2	130.52 (46.80)Aa2	149.25 (41.26)Aa2
Tan (δ)	0.42 (0.09)Aa	0.20 (0.05)Ba1	0.24 (0.06)Ba2	0.26 (0.07)Ab2	0.25 (0.03)Aa1	0.28 (0.06)Aa1	0.07 (0.01)Ac1	0.09 (0.02)Ab2	0.08 (0.02)Ab1

Abbreviations: TDg: Tideglusib; NPs: nanoparticles; LC: Load cycled; TC: Thermo-cycled E * (GPa): E * : Complex Modulus (GPa), *E''*: Loss Modulus (GPa), E´: Storage Modulus. Same capital letter indicates no significant difference between 24 h, load cycled and thermo-cycled groups, i.e, type of challenging, at the same interface zone and same experimental procedure. Identical lower case letter indicates no significant differences between different experimental procedure groups, i.e, similar type of challenging among the different groups. Same number indicates no significant differences between distinct zones within the same experimental procedure. Significance was set at $p < 0.05$.

achieved the highest resistance to dynamic deformation at the bottom of the hybrid layer, that corresponded with several discontinuous red collars in the mappings (Figs. 1A, 1B). In general terms, the control group achieved the lowest E * (Fig. 1D). Loss modulus *E''* performed similar in specimens treated with undoped NPs and TDg-NPs (Figs. S2B, S2D, respectively). Samples treated with any kind of NP and mechanically loaded attained the highest storage modulus *E'* (Figs. S3C, S3D). Tan (δ) practically performed similar in all groups (Table 1) (Fig. 2). At both intertubular and peritubular dentin, specimens infiltrated with any kind of NPs performed similar, showing the same E * , *E''*, *E'* and Tan (δ), regardless the type of challenging (Table 1).

Concerning the same type of challenging among different groups (lower case letters in Table 1), at the hybrid layer, specimens tested at 24 h showed the same E * , regardless the group of study (Fig. 1D). Samples treated with any kind of NPs and mechanically loaded had similar E * and performed superior than the control group. Specimens infiltrated with TDg-NPs thermo-cycled (Fig. 1C) achieved higher E * than the rest of the groups, that performed similar. Loss modulus *E''* and tan (δ) showed the same values at 24 h, and after both load and thermal cycling, when the three groups were compared (Fig. S4C). Storage modulus *E'* attained the same values at 24 h, and after both load and thermal cycling when the three groups were compared, except samples treated with undoped NPs that showed the highest values among groups (194.21 GPa) (Table 1) (Fig. S3C). At the bottom of the hybrid layer, the highest complex modulus E * was achieved by samples infiltrated with TDg-NPs, at 24 h storage. Samples treated with any kind of NPs and mechanically or thermal loaded had similar E * and performed superior than the control group. At 24 h storage and after load cycling, all samples showed similar loss modulus *E''* (Fig. S2). After thermo-cycling, samples treated with any kind of NPs had similar *E''* and performed superior than the control group. At 24 h storage, the highest storage modulus *E'* corresponded to specimens infiltrated with TDg-NPs (Fig. S3D). Samples treated with any kind of NPs and mechanically loaded had similar *E'* and performed superior than the control group (Fig. S3A). After thermo-cycling, all samples performed similar. All specimens showed the same tan (δ) at 24 h storage and after load cycling. Samples treated with any kind of NPs and thermically loaded had similar tan (δ) and performed superior than the control group (Fig. 2A).

At intertubular dentin, samples 24 h storage performed similar, showing the same E * values. After load cycling, specimens infiltrated with TDg-NPs showed the highest E * (Fig. 1B), and when samples were thermocycled they obtained similar E * . At 24 h of storage, samples treated with TDg-NPs attained the lowest loss modulus *E''* (Fig. S2C). The control group and samples treated with any kind of NPs, mechanically and thermically loaded achieved similar *E''*. At 24 h storage and mechanically loaded samples, all specimens attained the same storage modulus *E'*. Samples treated with any kind of NPs and thermically loaded achieved similar *E'* and performed superior than the control group (Fig. S3A). All specimens showed the same tan (δ), regardless the

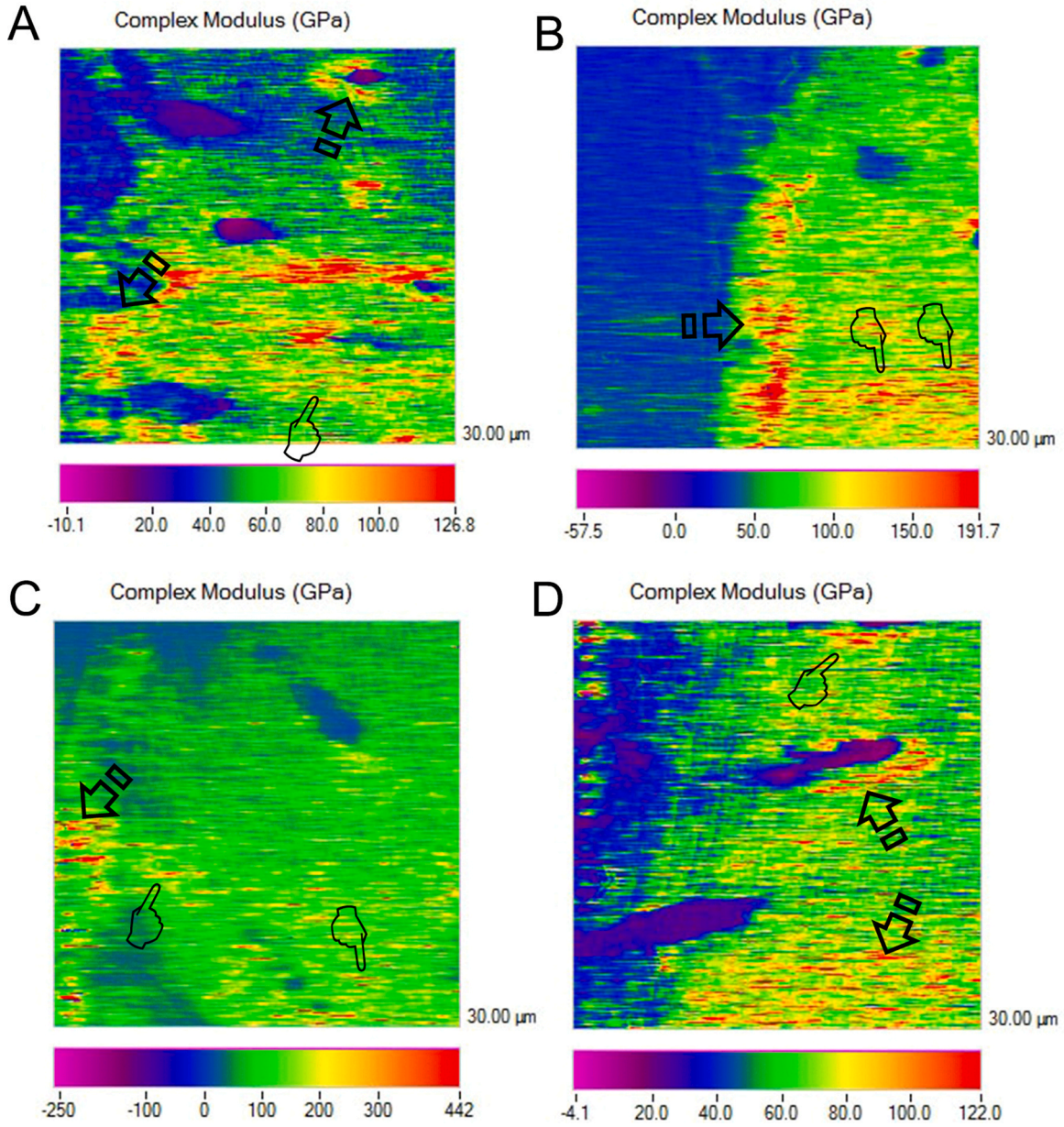

Fig. 1. Scanning mode nano-DMA analysis of the map of the complex modulus at the dentin infiltrated with undoped nanoparticles (NPs) in specimens load cycled (**A**), at dentin infiltrated with NPs doped with tideglusib (TDg-NPs) load cycled (**B**), at dentin infiltrated with NPs doped with tideglusib (TDg-NPs) thermo-cycled (**C**) and control group load cycled (**D**). In the color scheme shown, the dark color corresponds to lower values of the locally measured complex modulus E * . Discontinuous red collar point out areas of maximum E * (arrows). Closed loops in yellow to red traces signalize regions of maximum E * coinciding with peritubular viscoelasticity (pointers). Green zones within the red collar of high E * values suggest intratubular precipitation of crystals. Irregular blue circles spread out in the scan surface and most of them appeared framed by a collar of multiple red spots.

type of challenging (Table 1) (Fig. 2). At peritubular dentin, samples treated with any kind of NPs performed with similar E * , and superior than the control group at 24 h storage, after load cycling (Fig. 1D) and after thermo-cycling (Fig. 1C). At 24 h of storage and after load cycling, samples treated with TDg-NPs attained the lowest loss modulus *E″*. Samples treated with TDg-NPs and thermically loaded achieved the lowest *E″* (Fig. S2). All specimens showed the same storage modulus *E′* (Fig. S3), regardless the type of challenging. At 24 h storage, specimens infiltrated with TDg-NPs achieved the lowest tan (δ). After load cycling and thermo-cycling, specimens infiltrated with TDg-NPs achieved the lowest tan (δ) values (Table 1) (Figs. 2C, 2D).

Regarding the distinct zones within the same experimental procedure (numbers in Table 1), the control group specimens, regardless the subgroup (24 h storage, load cycling or thermo-cycling), exhibited the same E * throughout the resin-dentin interface without significant differences (Fig. 1D). Dentin infiltrated with undoped NPs, at 24 h storage, showed similar E * at both the HL and the BHL, and increased at intertubular dentin, attaining the highest complex modulus at peritubular dentin. Dentin infiltrated with undoped NPs, after load cycling, achieved the lowest E * at intertubular dentin, and significantly increased at peritubular dentin. Similar specimens, after thermo-cycling showed similar E * values at the interface, except at peritubular dentin, that increased their values. When demineralized dentin was infiltrated with TDg-NPs, samples stored for 24 h exhibited the same E * through the whole interface, but the HL had the lowest values (Fig. 1B). The groups infiltrated with both kind of NPs showed similar E * throughout the whole interface, regardless the type of challenging (Table 1).

Concerning the loss modulus *E″*, the highest values of the control

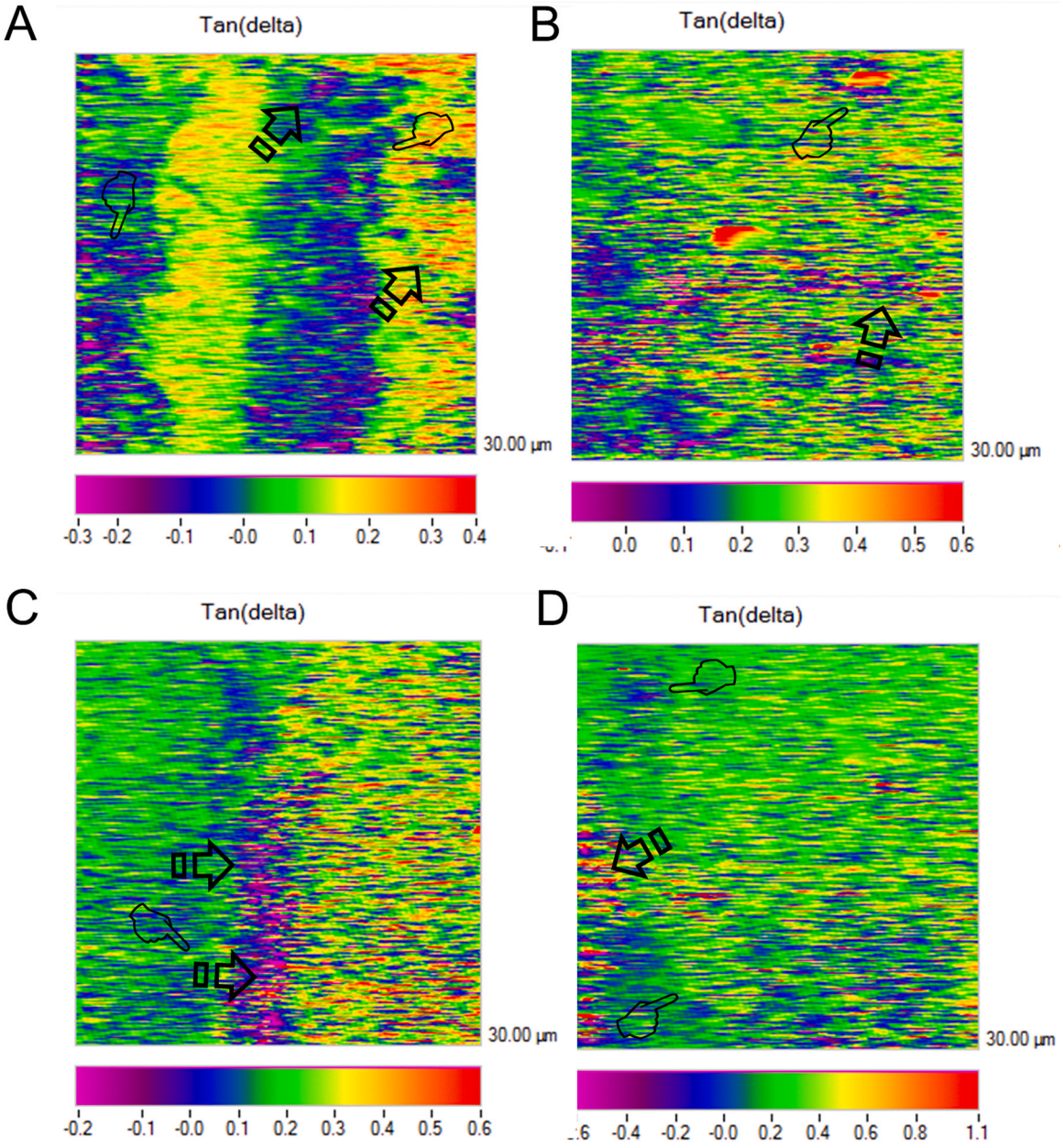

Fig. 2. Scanning mode nano-DMA analysis of the map of the tan (δ) at the control group thermo-cycled (**A**), at dentin infiltrated with undoped NPs load cycled (**B**), dentin infiltrated with NPs doped with tideglusib (TDg-NPs) load cycled (**C**) and dentin infiltrated with NPs doped with tideglusib (TDg-NPs) thermo-cycled (**D**). In the color scheme shown, the red color corresponds to the highest value of the locally tan (δ) value moduli, potentially associated to tan (δ) of intratubular and intertubular mineral precipitation (arrows). The capacity for getting rid of the energy at peritubular dentin is represented by the blue-green diffused marks (pointers), at the mapping.

group 24 h storage were obtained at peritubular dentin, and the rest of the interface performed similar. No changes were adverted after load cycling, and the highest values after thermo-cycling were achieved at intertubular dentin. Specimens with undoped NPs infiltration, regardless the type of challenging, showed similar E'' at the resin-dentin interface, but significantly increased at the peritubular dentin. Samples with TDg-NPs infiltration 24 h storage showed similar E'' throughout the resin-dentin interface (Fig. S2C). Those specimens, after load cycling, performed similar, but at the HL, E'' achieved the lowest values. After thermo-cycling the highest E'' values were obtained at the peritubular dentin (Table 1).

Respect to storage modulus E', samples of the control group 24 h storage and load cycled (Fig. S3A) exhibited higher E' at peritubular dentin than at intertubular dentin. After thermo-cycling, peritubular dentin achieved the highest E', but was not distinct to intertubular dentin. Demineralized dentin infiltrated with undoped NPs 24 h storage showed higher E' at peritubular dentin than at intertubular dentin. Both intertubular and peritubular dentin attained higher E' than both HL and BHL, after load cycling (Fig. S3C). After thermo-cycling, peritubular dentin attained the highest E' through the resin-dentin interface. After TDg-NPs, 24 h storage specimens showed the lowest E' at the hybrid layer. After load cycling, peritubular dentin exhibited higher E' than intertubular dentin. E' resulted similar after thermo-cycling (Table 1) (Fig. S3D).

Tan (δ) of control specimens load cycled did not change through the resin-dentin interface, but after thermo-cycling both hybrid layer and intertubular dentin attained the lowest values. Specimens treated with undoped NPs did not vary their tan (δ) regardless the typo of challenging

(Fig. 2B). Samples infiltrated with TDg-NPs, after load cycling, showed higher tan (δ) values at peritubular dentin than at intertubular dentin (Table 1) (Fig. S3C). The property map of the interface promoted by dentin infiltrated with undoped NPs and TDg-NPs both load cycled achieved the highest stored energy, mostly at HL and BHL in case of undoped NPs, and BHL and peritubular dentin in case of TDg-NPs and peritubular dentin (Figs. S3C, S3D).

3.2. Atomic Force Microscopy (AFM) analysis and collagen fibril diameter measurements

In the control group, resin dentin infiltration was observed at both peritubular and intertubular dentin at 24 h of storage. After load cycling, dentin tubules appeared occluded, but with mineralized peritubular dentin and some "bridging" processes. Located areas of mineralizarion were observed after thermo-cycling, and some other zones were not remineralized or scarcely mineralized (Fig. S4).

Some big processes of dentin remineralizarion were determined after 24 h of storage when demineralized dentin was infiltrated with undoped NPs. When these interfaces were load cycled, some samples showed breakdown zones at the interface, located at the limits between the peritubular and intertubular dentin, being parallel to the intratubular mineral deposits. Layered minerals which precipitated, preferentially, at intertubular dentin forming a consistent clump of crystals, were noticeable when dentin infiltrated with undoped NPs was thermo-cycled (Fig. 3).

Processes of intertubular and intratubular mineralization are taken place at interfaces of resin-dentin specimens infiltrated with TDg-NPs, and observed after 24 h of storage (Fig. 4A). Load cycling of these specimens permitted to perceive some stick-slip images, in radial direction, of nucleated minerals appearing as bridges and rod-like new mineral formations that surrounded the intratubular crystals. These precipitated crystals anchored the intratubular deposits of mineral to the peritubular dentin reducing the tubule entrances (Fig. 4B). These mineral beams remained attached, directly or indirectly through crack-bridging or bridging-like structures, likewise, when specimens were thermo-cycled (Fig. 4C).

Dentin specimens infiltrated with TDg-NPs showed the highest bandwidth among samples (Fig. 5). Most of the collagen fibrils exhibited their characteristics staggered pattern on the surface (Fig. S5).

4. Discussion

Resin-dentin interfaces promoted with both undoped NPs or TDg-NPs facilitated dentin crack formation after the dissipation of discrepant values of viscoelastic properties, but the presence of tideglusib favored the mineralization of the breakdown zones. Taking into account that both the loss modulus (E'') and the storage modulus (E') are implicated in the viscoelastic definition of the complex modulus (E *) and tan (δ), only E * and tan (δ) will be extensively discussed.

The highest values of complex modulus at both the hybrid layer (HL) and the bottom of the hybrid layer (BHL) were achieved when samples treated with undoped NPs or TDg-NPs were mechanically load cycled. Therefore, the first null hypothesis must be rejected. This greatest resistance to dynamic deformation, E * , that showed these two resin-dentin interfaces based on NPs dentin infiltration, is due to mineral precipitation at the intrafibrillar collagen of both HL and BHL [34]. Mineralization at the intrafibrillar collagen plays a crucial role in enhancing the mechanical properties performance [17]. The extrafibrillar minerals function as a granular material capable of withstand loads, especially in the lack of intrafibrillar mineralization. As a consequence, the second null hypothesis must, again, be rejected. Thereby, this absence is a crucial factor for predicting biomineralization [35]. Intermittent compressive loads have promoted mineralization in the present research and have enhanced alkaline phosphatase activity. Tissue alkaline phosphatase, existing at all mineralization locations, is a zinc-metalloenzyme that protects collagen [36], hydrolyzing a wide spectrum of phosphate monoesters [37]. This hydrolysis promotes apatite supersaturation [38], which facilitates the penetration of amorphous calcium phosphate into collagen. Calcium pyrophosphate plus non-crystalline amorphous and unstable complexes such as calcium phosphate finally are deposited under high phosphate concentrations around the collagen fibrils [39]. The present NPs perform as phosphate- and calcium- sequestering materials [11], functioning as biomimetic analogs that nucleate minerals [40] promoting dentin mineralization [12]. Polymeric NPs do not dissolve or reabsorb and are able to synthesize amorphous calcium phosphate layer at their surface, they endure bind to the collagen fibrils and are incorporated into the remineralized tissue [12]. The growth of calcium phosphate may be template by the carboxylate groups (COOH), as it has been beforehand proved in other diverse synthetic polymers [41,42]. The presence of NPs in the

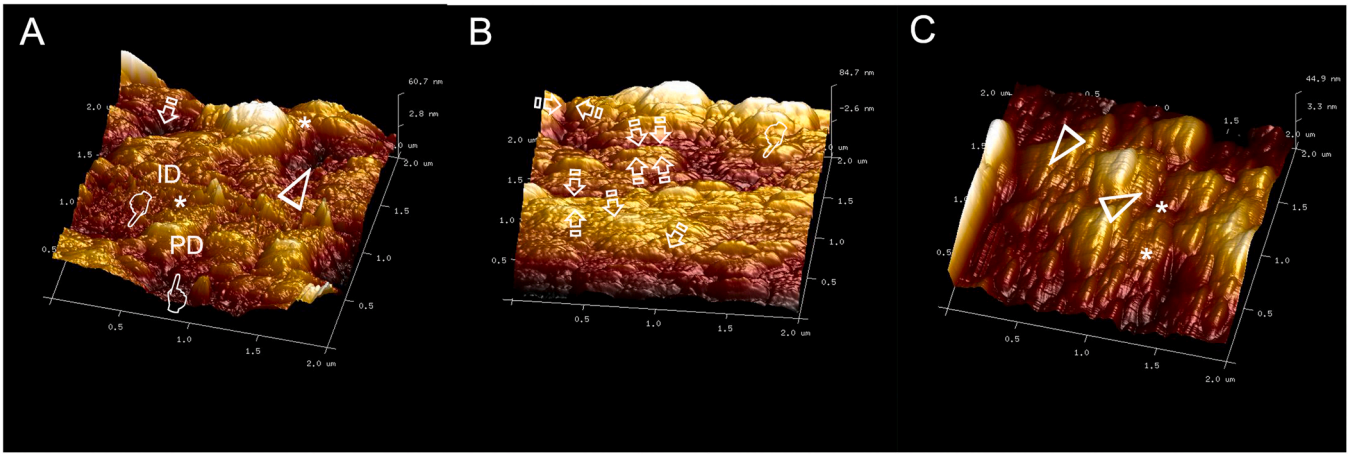

Fig. 3. Topography mapping of dentin obtained by AFM after applying undoped NPs, at 24 h time point (**A**). Some dentinal tubules appeared totally (pointers) or partially (arrowhead) mineral filled. Some other tubules were empty (arrow). Peritubular (PD) and intertubular dentin (ID) are clearly differentiated. Homogeneous transition between peritubular and intertubular dentin is evidenced (asterisks). (**B**), Nudes or mineral-integrated NPs, at both peritubular an intertubular locations, were observed (single arrows). The bond between the resin tag and the peritubular dentin was not perfect (pointer). The crack deflection and branching, around the peritubular cuff, may be observed at the dentinal wall of filled tubules (faced arrows) of dentin treated with undoped NPs, submitted to load cycling, showing clear neat stick-slip images as sight of energy dissipation. (**C**), Morphologically, homogeneous transition between peritubular and intertubular dentin characterizes the dentin surface (asterisks) in thermo-cycled specimens. Zones-free from breakdown were observed anywhere. Partially mineralized collagen fibbers may be observed (arrowheads).

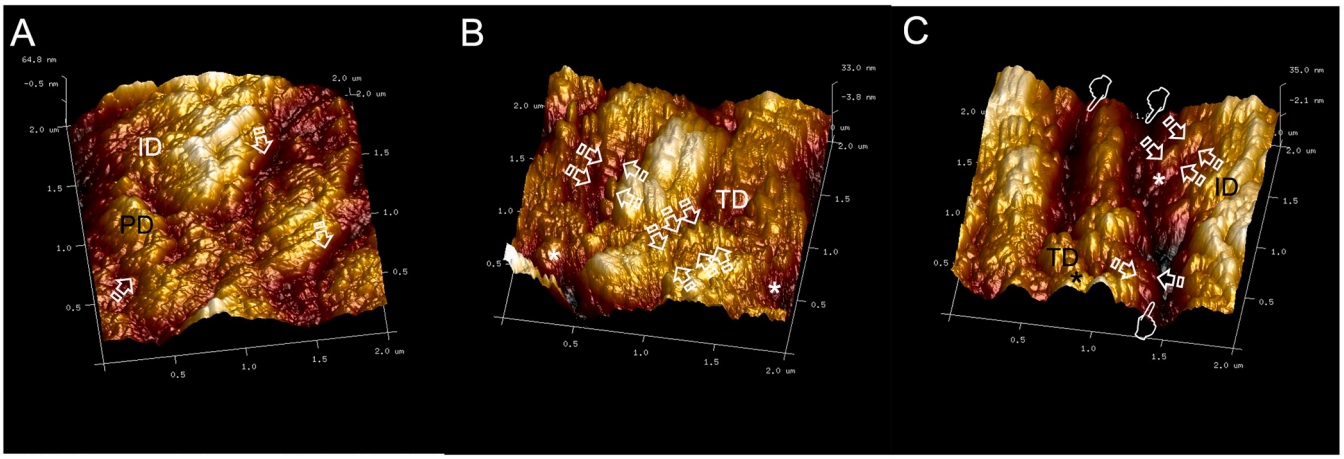

Fig. 4. Topography mapping of dentin obtained by AFM after applying TDg-NPs and 24 h time point (**A**). Peritubular (PD) and intertubular (ID) dentin mineralization is evident and open dentinal tubules are not observable (arrows). (**B**), After load cycling, intratubular dentin (TD) is totally occluding the dentinal tubules (asterisks). Stick-slip images and little rod-like minerals (faced arrows), as bridge-like structures indicating sight of energy dissipation at the limits between both PD and ID are present. (**C**), After thermocycling, NPs were scarcely observed, most of them covered by a layer of mineral (asterisks) that could not totally fill the tubule lumen (pointers). Little rod-like new minerals surrounding the intratubular crystals, directly or indirectly (faced arrows) anchored on the intratubular deposits of mineral to the peritubular dentin forming the "bridging" processes, limiting breakdown zones (asterisks).

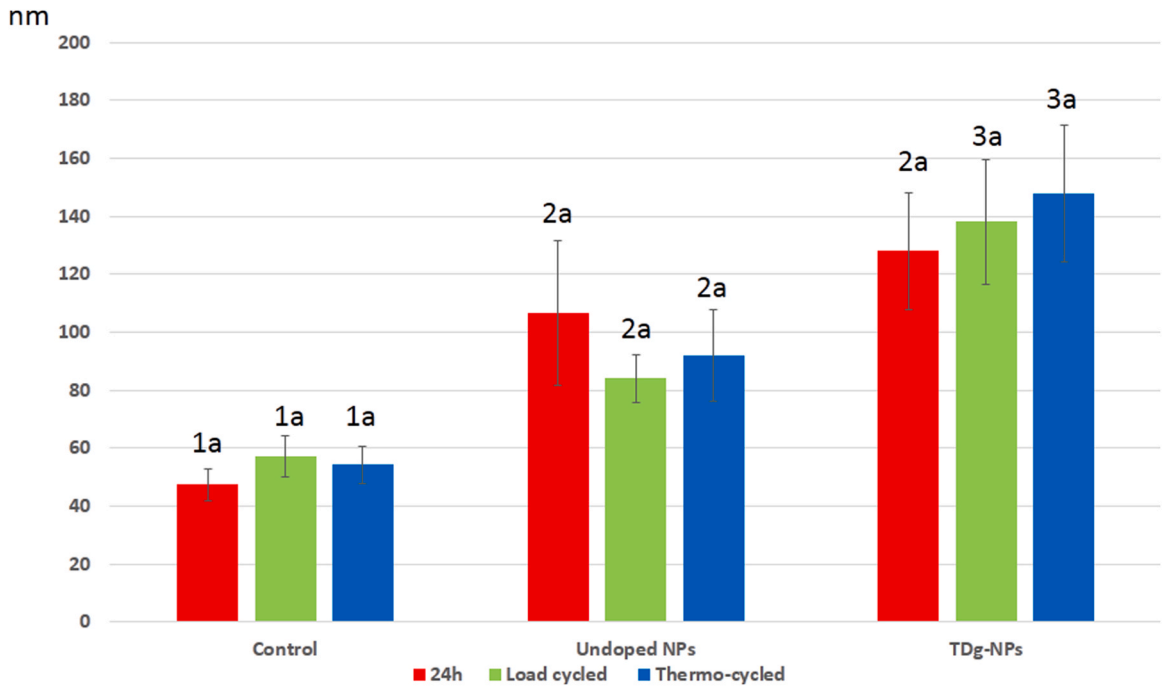

Fig. 5. Fibrils diameter at the different experimental resin-dentin interfaces. Identical lower case letters indicate no significant differences among samples treated with similar material. Identical numbers indicate no significant differences among distinct groups submitted to the same challenge. NPs, nanoparticles; TDg-NPs, Tideglusib doped NPs.

infiltrated collagen facilitated the dissipation of energy throughout the resin-dentin interface, as both hybrid layer and bottom of hybrid layer shared similar E * . TDg-NPs infiltration was dependent on the specific characteristics of the NPs [11,12]. Therefore, tested NPs have been previously characterized. They are spherical in shape and posse a hydrodynamic size of 250 nm (independently of their functionalization) [24,25]. Due to the negative zeta potential of NPs, they do not agglomerate [24].

Peritubular dentin has shown significantly higher E * than intertubular dentin (~1.5 fold) when undoped NPs were used and specimens were mechanically loaded (134.49 vs 87.62 GPa) (Table 1). Thereby, nano-DMA results have revealed, between peritubular and intertubular dentin, heterogeneity in the distribution of mechanical property after undoped NPs dentin infiltration in load cycled samples (Fig. 1A). Within the peritubular cuff, it means an increase of the energy concentration. Via deformation in radial and axial directions throughout a frictional pullout and bridging procedure, energy dissipation can occur at tubular structures. This process complies with mineral nucleation at micro and nano-scale planes [43]. The excess of energy, through cracking the dentin substrate, may be dissipated, interfering the energy transfer, affecting dentin remineralization and remodeling [44]. Red color reflected high E * values at peritubular locations (Fig. 1A). Clear circles of relevant values were exhibited by the complex modulus mapping, ranging from red to yellow intensities, being represented as diffuse

spheres septum-split in the majority of the figures. Therefore, discrepant properties of viscoelasticity at the distinct structures within the dentin, are a risk for the breakdown of this substrate, as in relatively high elastic modulus regions low modulus regions lead to energy concentration [2]. Both intertubular and peritubular dentin have been identified, scanning the interfaces, as the most pivotal junction in preventing crack generation and propagation throughout the boundary between the two different phases [45]. At the peritubular-intertubular dentin limit, the AFM topography image established the existence of a neat stick-slip image (Fig. 3B). These precipitates may be interpreted as frictional pullout, originated as a result of the discrepant viscoelastic outcomes between both structures [43].

On the contrary, when TDg-NPs were used to infiltrate dentin, after load cycling, E * at peritubular dentin was ~1.1 fold higher than intertubular dentin, but without significant differences (Table 1), revealing homogeneity in the mechanical feature distribution between intertubular and peritubular dentin, facilitating, thereby throughout their structures, the dissipation of the energy [43]. Nevertheless, tan (δ) at intertubular dentin of load cycled samples treated with TDg-NPs showed significant higher values (~2.9 fold) than at peritubular dentin. The ratio of the energy dissipated by the system to the energy stored in the system that enables its elastic recoil is equivalent to tan (δ). It assures how rightly a material can get rid of the energy [46]. The 3-D contour map of the tan (δ) distribution reflects this viscoelastic performance (Fig. 2C), showing close areas, i.e, intertubular and peritubular dentin, with opposite tan (δ) values. For recoil and/or failure, the lower tan (δ), the greater the proportion of energy available in the system [47]. Red intensity occupying most of the intertubular dentin area reflected this viscoelastic response (Fig. 2C). Intratubular mineral precipitation became potentially associated to the highest tan (δ) values, in the present study, promoting total occlusion of the dentinal tubules creating thick platforms of mineral (Fig. 4B). Dentin mechanical properties may be affected by occluded tubules. Microcracking of unfilled tubules (Fig. 3A, S2B) have been shown if compared with filled tubules, acting as uncracked-ligament bridging [44,48]. Minerals that precipitated are also observed at the intertubular-peritubular dentin limit (Fig. 4B). It has been established the existence of stick-slip figures at the intertubular-peritubular dentin edge, in specimens treated with TDg-NPs (Fig. 4). Besides, TDg-NPs infiltrated dentin, after mechanical (Fig. S5B) and thermal (Fig. S5C) cycling have promoted a significant increase of the fibrils width (Fig. 5), which commonly happens when cross-linking is maintained or intrafibrillar or functional mineralization exists [2,49]. TDg promotes dentin bridge formation [50]. At micro and nano-scale damage zones, nucleating minerals represented by these bridges of slipped mineralized dentin, might be influential in effectively resisting crack propagation and further fracture [44]. The stick-slips formation when TDg-NPs were applied on dentin, it is speculated that depends on the presence of tideglusib in the chemical formulation of the nanoparticle, which originated new crystals precipitation, making not possible to observe open dentinal tubules or demineralized collagen (Fig. 4). For this reason, it must be rejected the third null hypothesis. Surrounding the intratubular crystals and at peritubular dentin, these mineral precipitates were shown as multiple rod-like figures [38] (Figs. 4B, 4C), and they were absent in samples treated with undoped NPs analyzed after 24 h of storage (Fig. 3A), and also after thermo-cycling (Fig. 3C).

Different reasons have been advocated to explain the role of TDg in mineralization of hard tissues, as *i*) at the interface, the presence of the tested peptides may have inducted electrostatic attraction for the soluble ions, generating local increased of supersaturation zones that promote nucleation [51]; *ii*) distinct ligands that are existing in TDg such as hydroxyl groups, carboxyl, or carboxamide may bind to calcium [52]; *iii*) the collagen fiber stiffness may have increased due to the existence of the TDg loaded NPs in the resin-dentin interface, at the dentin extracellular matrix, thus causing a higher resistance to proteolysis of type I collagen fibers [14]; *iv*) besides, peritubular dentin preferentially absorbs some peptides, just the location where the remineralizing role has been advanced [53]. These findings are in agreement with the existence of new mineral deposits [9] at the resin-dentin interface and at the first 5–20 μm of the tubule dimensions [14].

At the HL, demineralized dentin infiltrated with TDg-NPs and thermo-cycled showed higher E * at the dentin interface than the specimens treated with undoped NPs. In general, load cycling promoted higher E * than thermo-cycling (Table 1) (Fig. 1B, 1C), with morphological implications (Fig. 4B, 4C). It confirms that mechanical loading facilitated intrafibrillar, biomimetic or functional remineralization [34], further than thermo-cycling. Noneless, after thermal cycling, the stimulation of alkaline phosphatase activity and proteins synthesis has been proved in vitro and in vivo [54], contributing to a reduction in exposed collagen [15], though associated to a non-functional mineralization [17].

The dentin specimens of the control group did show similar values of E * , regardless the different zones of the resin-dentin interface and the type of challenge (Table 1) (Fig. 1D). Nevertheless, the resistance to dynamic deformation, E * , attained generalized lower values than specimens treated with NPs-treated mechanically and thermo-mechanically loaded. Single Bond adhesive infiltrated at the phosphoric acid-conditioned dentin (control group) has been shown to exhibit high hydrophilicity at the resin-dentin interface, with excessive water adsorption and resin degradation. Even more, though adhesive resin infiltrated the intertubular dentin, many resin tags were absent, favoring nanoleakage and further degradation [55] (Fig. S2).

In relatively higher elastic modulus areas with low flexibility, lower storage modulus (E') regions with high flexibility conducts to stress concentration [47] and scarce dissipation of energy that favors breaking with failure at the resin-dentin interface [56]. Control specimens and those treated with TDg-NPs, after load cycling, attained an average increase of the storage modulus (E') at the peritubular dentin in comparison with the intertubular dentin of ~1.9 and 1.8 folds, respectively (Table 1), which was accompanied by mineral deposits at the peritubular-intertubular dentin limits, as confirmed both topographic mappings obtained by AFM. These precipitates appeared as bridge-like structures (Figs. S4A, 4B). A dispersed distribution of values with scarce resolution of the scans was revealed by the storage modulus map (Figs. S3A, S3D). Punctual red signals, simulating undefined circles of higher E', surrounded by lower E' results, were exhibited by the colored marks. Failure or fracture, from the stress distribution mapped by Misra et al. (2004) [2] could probably recruit at three different locations within the dentin and the hybrid layer (Fig. S1): *i*) at the interface between the adhesive tag and the peritubular dentin of the lumen wall due to stress concentration [57], *ii*), at the adhesive tag proximal to the hybrid layer due to stress concentration, *iii*), close to the bottom of the hybrid layer due to a high strain. Furthermore, if the bond between peritubular dentin and the adhesive tags is not perfect, as in Fig. 3B, then, within the hybrid layer the stress concentration zones are very likely to be focused, and the integrity of the resin-dentin interface will result damaged [58]. E' in samples treated with undoped NPs also showed higher average values at the peritubular dentin than at the intertubular dentin (~1.5 fold), but without significant differences (Table 1). Little rod-like minerals and stick-slip images were absent in specimens thermo-cycled (Fig. 3C).

This is to the best of our knowledge, the solely available results from AFM analysis and nano-DMA tests on tideglusib-doped NPs infiltrating the resin-dentin interface. Complementary techniques, such as SEM, TEM and XRD have yielded results that are in line with those obtained in the present research [14,59]. Thereby, this investigation poses the first try to measure the dentin ability to dissipate mechanical energy in function of the time-dependent behavior, in the presence of tideglusib. Nevertheless, the present study also has several shortcomings, as longer duration of thermal cycling, or selection of other bioactive ions and remineralizing agents into the chemical formula of the NPs. Other mechanical properties as fracture modulus and compressive modulus in

combination with studies of surface topography would have lengthened the message of this manuscript. The assessment of visible cracks would also contribute to the understanding of this mechanic-biology event. For an accurate mechanistic evaluation, the interpretation of the low-resolution of the mappings and the scanned images might introduce uncertainty concerning the contribution of the observed differences in the viscoelastic values at the resin-dentin interface among the tested groups. Future research should also be conducted to analyze by micro-computed tomography these rein-dentin bonded interfaces. The lack of this technique in this study may be considered as a limitation of the preset investigation.

5. Conclusions

The highest resistance to dynamic deformation at both the hybrid layer and the bottom of the hybrid layer was attained when specimens infiltrated with undoped nanoparticles or nanoparticles doped with tideglusib were mechanically load cycled, performing similar. Nano-DMA results revealed heterogeneity in the mechanical property distribution between peritubular and intertubular dentin after undoped nanoparticles dentin infiltration in samples submitted to load cycling, promoting frictional pullout between peritubular and intertubular dentin, due to stress concentration. Demineralized dentin infiltrated with nanoparticles doped with tideglusib and load cycled revealed homogeneity in the mechanical properties distribution between peritubular and intertubular dentin, facilitating, thereby, the dissipation of the energy throughout their structures when the complex modulus was assessed. Tan delta at both intertubular and peritubular dentin showed discrepant values, after load cycling of samples treated with TDg-doped nanoparticles, unveiling stick-slip images and multiple rod-like figures of mineral deposits mostly close to the peritubular dentin. This biomimetic mineralization occurred in collagen fibrils whose width resulted augmented after TDg infiltration.

Declaration of Competing Interest

The authors declare that they have no known competing financial interests or personal relationships that could have appeared to influence the work reported in this paper.

Acknowledgments

The present study was supported by Grant PID2020–114694RB-I00 funded by MCIN/AEI 10.13039/501100011033. This research is part of E. F-R.'s Ph.D. research study.Open Acess funding by Universidad de Granada / CBUA .

Appendix A. Supporting information

Supplementary data associated with this article can be found in the online version at doi:10.1016/j.dental.2024.09.005.

References

[1] Nakabayashi N, Pashley DH. Hybridization of Dental Hard Tissues. Quintessence Publishing Company; 1998.
[2] Misra A, Spencer P, Marangos O, Wang Y, Katz JL. Micromechanical analysis of dentin/adhesive interface by the finite element method. J Biomed Mater Res B Appl Biomater 2004;70B:56–65. https://doi.org/10.1002/jbm.b.30012.
[3] Toledano-Osorio M, Osorio R, Aguilera FS, Medina-Castillo AL, Toledano M, Osorio E, et al. Polymeric nanoparticles protect the resin-dentin bonded interface from cariogenic biofilm degradation. Acta Biomater 2020;111:316–26. https://doi.org/10.1016/j.actbio.2020.05.002.
[4] Hashimoto M, Ohno H, Sano H, Kaga M, Oguchi H. In vitro degradation of resin-dentin bonds analyzed by microtensile bond test, scanning and transmission electron microscopy. Biomaterials 2003;24:3795–803. https://doi.org/10.1016/s0142-9612(03)00262-x.
[5] Hebling J, Pashley DH, Tjäderhane L, Tay FR. Chlorhexidine arrests subclinical degradation of dentin hybrid layers in vivo. J Dent Res 2005;84:741–6. https://doi.org/10.1177/154405910508400811.
[6] Pashley DH, Tay FR, Yiu C, Hashimoto M, Breschi L, Carvalho RM, et al. Collagen degradation by host-derived enzymes during aging. J Dent Res 2004;83:216–21. https://doi.org/10.1177/154405910408300306.
[7] Breschi L, Mazzoni A, Nato F, Carrilho M, Visintini E, Tjäderhane L, et al. Chlorhexidine stabilizes the adhesive interface: a 2-year in vitro study. Dent Mater 2010;26:320–5. https://doi.org/10.1016/j.dental.2009.11.153.
[8] Carrilho MR, Tay FR, Donnelly AM, Agee KA, Tjäderhane L, Mazzoni A, et al. Host-derived loss of dentin matrix stiffness associated with solubilization of collagen. J Biomed Mater Res B Appl Biomater 2009;90:373–80. https://doi.org/10.1002/jbm.b.31295.
[9] Profeta AC, Mannocci F, Foxton R, Watson TF, Feitosa VP, De Carlo B, et al. Experimental etch-and-rinse adhesives doped with bioactive calcium silicate-based micro-fillers to generate therapeutic resin–dentin interfaces. Dent Mater 2013;29:729–41. https://doi.org/10.1016/j.dental.2013.04.001.
[10] Thadathil Varghese J, Islam F, Farrar P, Prentice L, Prusty BG. Multi-response optimisation analysis of material properties in dental restorative composites under the influence of thermal and thermomechanical stimuli - a 3D finite element study. J Mech Behav Biomed Mater 2024;150:106363. https://doi.org/10.1016/j.jmbbm.2023.106363.
[11] Besinis A, van Noort R, Martin N. Remineralization potential of fully demineralized dentin infiltrated with silica and hydroxyapatite nanoparticles. Dent Mater 2014;30:249–62. https://doi.org/10.1016/j.dental.2013.11.014.
[12] Osorio R, Osorio E, Medina-Castillo AL, Toledano M. Polymer nanocarriers for dentin adhesion. J Dent Res 2014;93:1258–63. https://doi.org/10.1177/0022034514551608.
[13] Neves VCM, Babb R, Chandrasekaran D, Sharpe PT. Promotion of natural tooth repair by small molecule GSK3 antagonists. Sci Rep 2017;7:39654. https://doi.org/10.1038/srep39654.
[14] Toledano M, Aguilera FS, Fernández-Romero E, Lagos AJ, Bonilla M, Lynch CD, et al. Dentin remineralization using a stimuli-responsive engineered small molecule GSK3 antagonists-functionalized adhesive. Dent Mater 2024;40:393–406. https://doi.org/10.1016/j.dental.2023.12.010.
[15] Balooch M, Habelitz S, Kinney JH, Marshall SJ, Marshall GW. Mechanical properties of mineralized collagen fibrils as influenced by demineralization. J Struct Biol 2008;162:404–10. https://doi.org/10.1016/j.jsb.2008.02.010.
[16] Li Y, Thula TT, Jee S, Perkins SL, Aparicio C, Douglas EP, et al. Biomimetic mineralization of woven bone-like nanocomposites: role of collagen cross-links. Biomacromolecules 2012;13:49–59. https://doi.org/10.1021/bm201070g.
[17] Bertassoni LE, Habelitz S, Kinney JH, Marshall SJ, Marshall Jr GW. Biomechanical perspective on the remineralization of dentin. Caries Res 2009;43:70–7. https://doi.org/10.1159/000201593.
[18] Poon B, Rittel D, Ravichandran G. An analysis of nanoindentation in linearly elastic solids. Int J Solids Struct 2008;45:6018–33. https://doi.org/10.1016/j.ijsolstr.2008.07.021.
[19] Hu S, Li J, Liu L, Dai R, Sheng Z, Wu X, et al. Micro/nanostructures and mechanical properties of trabecular bone in ovariectomized rats. Int J Endocrinol 2015;2015:e252503. https://doi.org/10.1155/2015/252503.
[20] Bar-On B, Daniel Wagner H. Elastic modulus of hard tissues. J Biomech 2012;45:672–8. https://doi.org/10.1016/j.jbiomech.2011.12.003.
[21] Ryou H, Romberg E, Pashley DH, Tay FR, Arola D. Importance of age on the dynamic mechanical behavior of intertubular and peritubular dentin. J Mech Behav Biomed Mater 2015;42:229–42. https://doi.org/10.1016/j.jmbbm.2014.11.021.
[22] Wilkinson TM, Zargari S, Prasad M, Packard CE. Optimizing nano-dynamic mechanical analysis for high-resolution, elastic modulus mapping in organic-rich shales. J Mater Sci 2015;50:1041–9. https://doi.org/10.1007/s10853-014-8682-5.
[23] Hayot CM, Forouzesh E, Goel A, Avramova Z, Turner JA. Viscoelastic properties of cell walls of single living plant cells determined by dynamic nanoindentation. J Exp Bot 2012;63:2525–40. https://doi.org/10.1093/jxb/err428.
[24] Toledano-Osorio M, Osorio E, Aguilera FS, Luis Medina-Castillo A, Toledano M, Osorio R. Improved reactive nanoparticles to treat dentin hypersensitivity. Acta Biomater 2018;72:371–80. https://doi.org/10.1016/j.actbio.2018.03.033.
[25] Medina-Castillo AL. Thermodynamic principles of precipitation polymerization and role of fractal nanostructures in the particle size control. Macromolecules 2020;53:5687–700. https://doi.org/10.1021/acs.macromol.0c00973.
[26] Sauro S, Mannocci F, Toledano M, Osorio R, Pashley DH, Watson TF. EDTA or H3PO4/NaOCl dentine treatments may increase hybrid layers' resistance to degradation: a microtensile bond strength and confocal-micropermeability study. J Dent 2009;37:279–88. https://doi.org/10.1016/j.jdent.2008.12.002.
[27] Han L, Grodzinsky AJ, Ortiz C. Nanomechanics of the cartilage extracellular matrix. Annu Rev Mater Res 2011;41:133–68. https://doi.org/10.1146/annurev-matsci-062910-100431.
[28] Hertz H. Über die Berührung fester elastischer Körper. J Reine Angew Math 1881;92:156.
[29] Macosko C.W. Rheology principles. Meas Appl 1994.
[30] Ryou H, Niu L-N, Dai L, Pucci CR, Arola DD, Pashley DH, et al. Effect of biomimetic remineralization on the dynamic nanomechanical properties of dentin hybrid layers. J Dent Res 2011;90:1122–8. https://doi.org/10.1177/0022034511414059.
[31] Pashley DH, Tay FR, Carvalho RM, Rueggeberg FA, Agee KA, Carrilho M, et al. From dry bonding to water-wet bonding to ethanol-wet bonding. A review of the interactions between dentin matrix and solvated resins using a macromodel of the hybrid layer. Am J Dent 2007:20.

[32] Habelitz S, Balooch M, Marshall SJ, Balooch G, Marshall GW. In situ atomic force microscopy of partially demineralized human dentin collagen fibrils. J Struct Biol 2002;138:227–36. https://doi.org/10.1016/s1047-8477(02)00029-1.
[33] Takeyasu K, Omote H, Nettikadan S, Tokumasu F, Iwamoto-Kihara A, Futai M. Molecular imaging of Escherichia coli F0F1-ATPase in reconstituted membranes using atomic force microscopy. FEBS Lett 1996;392:110–3. https://doi.org/10.1016/0014-5793(96)00796-x.
[34] Kinney JH, Habelitz S, Marshall SJ, Marshall GW. The importance of intrafibrillar mineralization of collagen on the mechanical properties of dentin. J Dent Res 2003;82:957–61. https://doi.org/10.1177/154405910308201204.
[35] Qin C, Brunn JC, Cadena E, Ridall A, Tsujigiwa H, Nagatsuka H, et al. The expression of dentin sialophosphoprotein gene in bone. J Dent Res 2002;81:392–4. https://doi.org/10.1177/154405910208100607.
[36] Patil P, Banga KS, Pawar AM, Pimple S, Ganeshan R. Influence of root canal obturation using gutta-percha with three different sealers on root reinforcement of endodontically treated teeth. An in vitro comparative study of mandibular incisors. J Conserv Dent 2017;20:241. https://doi.org/10.4103/JCD.JCD_233_16.
[37] Brosh T, Metzger Z, Pilo R. Circumferential root strains generated during lateral compaction with stainless steel vs. nickel-titanium finger spreaders. Eur J Oral Sci 2018;126:518–25. https://doi.org/10.1111/eos.12569.
[38] Toledano M, Osorio R, Osorio E, Medina-Castillo AL, Toledano-Osorio M, Aguilera FS. Ions-modified nanoparticles affect functional remineralization and energy dissipation through the resin-dentin interface. J Mech Behav Biomed Mater 2017;68:62–79. https://doi.org/10.1016/j.jmbbm.2017.01.026.
[39] Sui T, Sandholzer MA, Baimpas N, Dolbnya IP, Walmsley A, Lumley PJ, et al. Multiscale modelling and diffraction-based characterization of elastic behaviour of human dentine. Acta Biomater 2013;9:7937–47. https://doi.org/10.1016/j.actbio.2013.04.020.
[40] Watson TF, Atmeh AR, Sajini S, Cook RJ, Festy F. Present and future of glass-ionomers and calcium-silicate cements as bioactive materials in dentistry: biophotonics-based interfacial analyses in health and disease. Dent Mater 2014;30:50–61. https://doi.org/10.1016/j.dental.2013.08.202.
[41] Li Y, Aparicio C. Discerning the subfibrillar structure of mineralized collagen fibrils: a model for the ultrastructure of bone. PloS One 2013;8:e76782. https://doi.org/10.1371/journal.pone.0076782.
[42] Song J, Malathong V, Bertozzi CR. Mineralization of synthetic polymer scaffolds: a bottom-up approach for the development of artificial bone. J Am Chem Soc 2005;127:3366–72. https://doi.org/10.1021/ja043776z.
[43] Agrawal R, Nieto A, Chen H, Mora M, Agarwal A. Nanoscale damping characteristics of boron nitride nanotubes and carbon nanotubes reinforced polymer composites. ACS Appl Mater Interfaces 2013;5:12052–7. https://doi.org/10.1021/am4038678.
[44] Shinno Y, Ishimoto T, Saito M, Uemura R, Arino M, Marumo K, et al. Comprehensive analyses of how tubule occlusion and advanced glycation end-products diminish strength of aged dentin. Sci Rep 2016;6:19849. https://doi.org/10.1038/srep19849.
[45] Marshall GW, Habelitz S, Gallagher R, Balooch M, Balooch G, Marshall SJ. Nanomechanical Properties of Hydrated Carious Human Dentin. J Dent Res 2001;80:1768–71. https://doi.org/10.1177/00220345010800081701.
[46] Espino DM, Shepherd DE, Hukins DW. Viscoelastic properties of bovine knee joint articular cartilage: dependency on thickness and loading frequency. BMC Musculoskelet Disord 2014;15:205. https://doi.org/10.1186/1471-2474-15-205.
[47] Gopalakrishnan V, Zukoski CF. Delayed flow in thermo-reversible colloidal gels. J Rheol 2007;51:623–44. https://doi.org/10.1122/1.2736413.
[48] Koester KJ, Ager JW, Ritchie RO. The effect of aging on crack-growth resistance and toughening mechanisms in human dentin. Biomaterials 2008;29:1318–28. https://doi.org/10.1016/j.biomaterials.2007.12.008.
[49] Bertassoni LE, Habelitz S, Pugach M, Soares PC, Marshall SJ, Marshall GW. Evaluation of surface structural and mechanical changes following remineralization of dentin. Scanning 2010;32:312–9. https://doi.org/10.1002/sca.20199.
[50] Kornsuthisopon C, Tompkins KA, Osathanon T. Tideglusib enhances odontogenic differentiation in human dental pulp stem cells in vitro. Int Endod J 2023;56:369–84. https://doi.org/10.1111/iej.13877.
[51] Gungormus M, Tulumbaci F. Peptide-assisted pre-bonding remineralization of dentin to improve bonding. J Mech Behav Biomed Mater 2021;113:104119. https://doi.org/10.1016/j.jmbbm.2020.104119.
[52] Carvalho RG, Patekoski LF, Puppin-Rontani RM, Nakaie CR, Nascimento FD, Tersariol ILS. Self-assembled peptide P11-4 interacts with the type I collagen C-terminal telopeptide domain and calcium ions. Dent Mater 2023;39:708–17. https://doi.org/10.1016/j.dental.2023.06.004.
[53] Moussa DG, Kirihara JA, Ye Z, Fischer NG, Khot J, Witthuhn BA, et al. Dentin priming with amphipathic antimicrobial peptides. J Dent Res 2019;98:1112–21. https://doi.org/10.1177/0022034519863772.
[54] Lozupone E, Palumbo C, Favia A, Ferretti M, Palazzini S, Cantatore FP. Intermittent compressive load stimulates osteogenesis and improves osteocyte viability in bones cultured “in vitro. Clin Rheuma 1996;15:563–72. https://doi.org/10.1007/BF02238545.
[55] Tay FR, Pashley DH. Have dentin adhesives become too hydrophilic? J Can Dent Assoc 2003;69:726–31.
[56] Angker L, Swain MV. Nanoindentation: application to dental hard tissue investigations. J Mater Res 2006;21:1893–905. https://doi.org/10.1557/jmr.2006.0257.
[57] Misra A, Spencer P, Marangos O, Wang Y, Katz JL. Parametric study of the effect of phase anisotropy on the micromechanical behaviour of dentin–adhesive interfaces. J R Soc Interface 2005;2:145–57. https://doi.org/10.1098/rsif.2005.0029.
[58] Toledano M, Osorio E, Cabello I, Aguilera FS, López-López MT, Toledano-Osorio M, et al. Nanoscopic dynamic mechanical analysis of resin–infiltrated dentine, under in vitro chewing and bruxism events. J Mech Behav Biomed Mater 2016;54:33–47. https://doi.org/10.1016/j.jmbbm.2015.09.003.
[59] Toledano M, Fernández-Romero E, Osorio MT, Osorio E, Aguilera FS, Toledano R, et al. Investigation of the effect of Tideglusib on the hydroxyapatite formation, crystallinity and elasticity of conditioned resin-dentin interfaces. J Dent 2024;150:105334. https://doi.org/10.1016/j.jdent.2024.105334.